

Continuum model of irradiation-induced spinodal decomposition in the presence of dislocationsJ. J. Hoyt¹ and M. Haataja²¹*Department of Materials Science and Engineering, McMaster University, Hamilton, Ontario, Canada L8S4L7*²*Department of Mechanical and Aerospace Engineering, Princeton Institute for the Science and Technology of Materials (PRISM), Program in Applied and Computational Mathematics (PACM), Princeton University, Princeton, New Jersey 08544*

(Received 30 January 2011; revised manuscript received 28 March 2011; published 11 May 2011)

A model of phase-separation kinetics in systems exposed to energetic particle irradiation has been extended to include the effects of mobile dislocations. It is shown that when dislocations are allowed to participate in the decomposition reaction, phase separation can occur at temperatures above the coherent spinodal, which is in agreement with several experiments on irradiated alloys. A linear stability analysis of the governing kinetic equations is performed and three regimes of microstructural evolution are identified within the parameter space of damage cascade size vs incident flux: complete phase separation, solid-solution behavior, and compositional patterning. In addition, numerical simulations of the evolving dislocation density and composition fields are performed. The numerical results provide the amplitude and wavelength of the stable patterns that can form under irradiation and elucidate the role of misfit dislocations in reducing the coherency strain due to atomic size mismatch.

DOI: [10.1103/PhysRevB.83.174106](https://doi.org/10.1103/PhysRevB.83.174106)

PACS number(s): 61.82.Bg, 61.72.-y, 64.75.Op

I. INTRODUCTION

In alloys exposed to a flux of energetic ions, electrons, or neutrons, the phase equilibrium and phase transformation behavior can be quite different from that observed in the absence of irradiation.¹ As shown experimentally for the case of Ge precipitates in Al-Ge alloys,² the generation of excess vacancies and mobile interstitials from damage cascade events can enhance the kinetics of nucleation.³ In other instances, however, irradiation damage can lead to the dissolution of particles and/or the stagnation of precipitate coarsening.⁴⁻⁸ Furthermore, irradiation can lead to the formation of incoherent precipitates of phases that do not appear on the equilibrium phase diagram⁹ and for the case of coherent precipitation, Cauvin and Martin have shown both experimentally¹⁰ and theoretically¹¹ that irradiation effects can lead to nucleation in undersaturated solid solutions. In addition to changes in nucleation and growth behavior, irradiation, in the case of order-disorder reactions, can change the qualitative nature of the transition. Not only can phase stability be altered under irradiation conditions,¹² but second-order transitions can become first order above a critical ballistic mixing flux.^{13,14}

Spinodal decomposition, or the initial stages of phase separation following a quench into the unstable region of the temperature-composition equilibrium diagram, also has been studied extensively for alloys under irradiation. A small-angle neutron-scattering experiment on Ni-Cu by Wagner *et al.*¹⁵ has shown that the increased solute mobility arising from electron irradiation leads to spinodal decomposition at temperatures where diffusivities under thermal conditions are extremely low. A similar mechanism has been suggested for phase separation in the case of Fe-Ni alloys.¹⁶ Perhaps the most comprehensive investigation of irradiation-induced spinodal decomposition is the work of Nakai, Kinoshita, and co-workers¹⁷⁻¹⁹ who have studied various compositions of Au-Ni, Cu-Ni, and Fe-Mo alloys using transmission electron microscopy. A particularly striking result of the Nakai *et al.* experiments is the observation that under irradiation, phase separation can occur at temperatures far above the coherent spinodal. The authors

attribute the seemingly contradictory result of unstable growth within the stable region of the phase diagram to fluctuations in the composition of excess point defects, which occur over the same length scale as the solute composition field and which act to relieve the coherency strain arising from atomic size mismatch. However, Nakai *et al.* offer no quantitative model for their proposed mechanism and in the present work we suggest an alternative explanation. The excess point defects generated during a cascade can provide sufficient mobility to dislocations such that strain relieving misfit dislocations move in concert with the concentration field during phase evolution. A continuum model of a mobile dislocation density field has been formulated by Haataja and co-workers²⁰⁻²² and indeed Leonard and Haataja²³ have shown that phase separation can take place above the coherent spinodal if dislocations are allowed to participate in the process. Some qualitative experimental evidence for a defect-assisted spinodal decomposition mechanism has been provided by Asai *et al.*¹⁹ who observed periodic arrays of interstitial loops in Au-Ni with a period coincident with the spatial variation in solute concentration.

In a series of papers Enrique and Bellon²⁴⁻²⁸ have demonstrated that for phase separating systems, microstructural evolution under the influence of ballistic mixing effects from energetic particles can exhibit a wide range of behavior depending on the irradiation conditions. The spatial extent of the cascade region, a function of the energy of incident particles, introduces an additional length scale in the problem, which can compete with the length scale established by the wavelength of the fastest growing composition modulation found from the linear theory of spinodal decomposition. Similarly, the time scale arising from the flux of incident particles can compete with the time scale of solute diffusion. The complex interaction between the time and length scales leads to three distinct regimes in parameter space: a region where a solid solution is maintained, a region where normal macroscopic phase separation is observed, and an intermediate case where a uniform solid solution is unstable, yet complete phase separation does not occur. The latter

region is characterized by a steady-state composition pattern where the dominant concentration wavelength and amplitude are unchanged with time. It is of interest to note that the aforementioned experiments of Nakai *et al.* have found a time-independent concentration amplitude.

The purpose of the present work is to extend the Enrique-Bellon model to include the effects of mobile dislocations. In the next section we establish the equations governing the time evolution of both the concentration field and the dislocation density field for a system under irradiation. In the subsequent section we perform a linear stability analysis and investigate how the regime of macroscopic phase separation, solid solution, and patterning are influenced by such materials parameters as dislocation mobility, temperature, solute-dislocation coupling, and dislocation core energy. Also in the results section, we will present numerical solutions to the kinetic equations and compare microstructures for systems within and outside the patterning region. The final section summarizes the conclusions of this work.

II. THEORETICAL BACKGROUND

The starting point for the description of dislocation-assisted spinodal decomposition under irradiation conditions is a model for the free energy of the binary alloy. The free energy can be written as a sum of four separate terms:

$$F = F_{\text{chem}} + F_b + F_{\text{coup}} + F_{\text{ball}}. \quad (1)$$

For the chemical contribution, the first term on the right-hand side of Eq. (1), we will adopt the Cahn-Hilliard²⁹ formulation given by

$$F_{\text{chem}} = \int d\mathbf{x} \left[-\frac{a}{2} \left(1 - \frac{\tilde{\eta}^2 E}{a} \right) c^2 + \frac{h}{4} c^4 + \frac{\epsilon^2}{2} |\nabla c|^2 \right], \quad (2)$$

where c is the concentration minus the overall average composition of the alloy and ϵ^2 is the gradient energy coefficient. The parameters a and h are constants describing the double-well free energy of a homogeneous system; a is negative for temperatures above the chemical spinodal and $a > 0$ for temperatures within the region of instability with respect to composition. In Eq. (2) the coherency strains due to atomic size mismatch are captured by the term containing Young's modulus E and the parameter $\tilde{\eta}$, which is the relative change in the lattice parameter with respect to the composition and is defined by $l = l_0(1 + \tilde{\eta}c)$ with l_0 being the lattice parameter for an alloy of average concentration³⁰ (see also Ref. 31). The elastic energy contribution employed here differs from that originally derived by Cahn because we are assuming a two-dimensional rather than a three-dimensional system (see Appendix A). The elastic strain energy determines the coherent spinodal as the point at which $a - \tilde{\eta}^2 E = 0$ and illustrates the fact that larger values of a , i.e., deeper quenches, are required to overcome the stabilizing effect of coherency strains.

Dislocation-dislocation interactions are incorporated in the model through the F_b term. Following Haataja *et al.* we can write

$$F_b = \int d\mathbf{x} \left[\frac{\alpha}{2} |\tilde{b}|^2 + \frac{1}{2E} (\nabla^2 \tilde{X}_d)^2 \right], \quad (3)$$

where α describes the core energy of the dislocations. Let \tilde{b}_x and \tilde{b}_y represent the x and y components of the continuous dislocation density field and confine the discussion to a two-dimensional system. Then the elastic strain energy of the system is governed by the Airy's stress function \tilde{X}_d , which must satisfy

$$\nabla^4 \tilde{X}_d = E(\nabla_x \tilde{b}_y - \nabla_y \tilde{b}_x). \quad (4)$$

The third term on the right-hand side of Eq. (1) describes the coupling between the solute concentration and the strain field of the dislocations. As shown in Appendix A, the F_{coup} contribution can be written as

$$F_{\text{coup}} = \tilde{\eta} \int d\mathbf{x} c \nabla^2 \tilde{X}_d, \quad (5)$$

where $\tilde{\eta}$ has been defined above. The dislocation model described above has also been used (albeit without the composition effect) in a study of two-dimensional melting by Nelson and co-workers^{32,33} and more recently by Bako and Hoffelner³⁴ (see also Ref. 35) in a theoretical study of dislocation patterning during plastic deformation. In addition, Enomoto and Iwata³⁶ have employed a similar approach to model phase separation in misfitting binary thin films.

Finally, for the free energy increase due to ballistic mixing of atoms arising from irradiation cascade events we will use the model developed by Enrique and Bellon:

$$F_{\text{ball}} = \frac{\Gamma}{2M} \int d\mathbf{x} c(\mathbf{x}) \int d\mathbf{x}' g(\mathbf{x} - \mathbf{x}') c(\mathbf{x}'). \quad (6)$$

Here Γ is the flux of energetic particles and M denotes the solute mobility. Furthermore, the function g is a kernel satisfying

$$\nabla^2 g(\mathbf{x} - \mathbf{x}') = -[\delta(\mathbf{x} - \mathbf{x}') - w_R(\mathbf{x} - \mathbf{x}')]. \quad (7)$$

The term w_R is a weighting function that describes the spatial extent of ballistic exchanges under irradiation conditions and is normalized such that the integral of w_R over all space is unity. Enrique and Bellon chose a Yukawa potential for the weight function. The Yukawa form is both a fairly accurate description of irradiation effects in crystals and allows for an analytic linearized formulation, in Fourier space, of the ballistic mixing contribution. Therefore, in the present work we will adopt the two-dimensional analog of the Yukawa potential, which can be written as

$$w_R(x) = \frac{1}{2\pi R^2} K_0(x/R), \quad (8)$$

where K_0 is the modified Bessel function of order zero. The radius R appearing in the weighting function represents the spatial extent of the cascade event and is a function of the energy of the incident particle. As alluded to in the Introduction, R and Γ are length and time scales due to irradiation effects that compete with the wavelength of the fastest growing concentration fluctuation according to the linear theory of spinodal decomposition and the solute mobility M . Enomoto and Sawa³⁷ have investigated a Gaussian weight function rather than a Yukawa potential and found qualitatively similar behavior to the Enrique-Bellon results.

The kinetics of the conserved c , \tilde{b}_x , and \tilde{b}_y fields can be established from the free-energy formulations of Eqs. (1) and (2)–(6):

$$\frac{\partial c}{\partial t} = M \nabla^2 \frac{\delta F}{\delta c}, \quad (9)$$

$$\frac{\partial \tilde{b}_x}{\partial t} = (M_g \nabla_x^2 + M_c \nabla_y^2) \frac{\delta F}{\delta \tilde{b}_x}, \quad (10)$$

$$\frac{\partial \tilde{b}_y}{\partial t} = (M_c \nabla_x^2 + M_g \nabla_y^2) \frac{\delta F}{\delta \tilde{b}_y}. \quad (11)$$

In the above formulation we have neglected contributions due to thermal noise.

Before proceeding, it is convenient to cast all variables into dimensionless form. The scaled variables are found from:

$$\mathbf{r} = \left(\frac{\epsilon^2}{a}\right)^{-1/2} \mathbf{x}, \quad u = \left(\frac{a}{h}\right)^{-1/2} c, \quad X_d = \left(\frac{E\epsilon^4}{h}\right)^{-1/2} \tilde{X}_d, \\ \mathbf{b} = \left(\frac{a^3}{E\epsilon^2 h}\right)^{-1/2} \tilde{\mathbf{b}}, \quad m_{c,g} = \frac{M_{c,g}\epsilon^2 E}{Ma^2}.$$

With the above definitions and an evaluation of the variational derivatives in Eq. (11),³⁸ the following equations governing the composition and dislocation density fields are established:

$$\frac{\partial u}{\partial \tau} = \nabla^2 [-(1-\eta)u + u^3 - \nabla^2 u] + \eta \nabla^4 X_d \\ - \gamma \int d\mathbf{r}' [\delta(\mathbf{r} - \mathbf{r}') - w_R(\mathbf{r} - \mathbf{r}')] u(\mathbf{r}'), \quad (12)$$

$$\frac{\partial b_x}{\partial \tau} = (m_g \nabla_x^2 + m_c \nabla_y^2) \\ \times \left[\nabla_y X_d + \eta \nabla_y \int d\mathbf{r}' G(\mathbf{r}, \mathbf{r}') \nabla_{\mathbf{r}'}^2 u + e b_x \right], \quad (13)$$

and an analogous equation arises for b_y , but with ∇_y replaced by $-\nabla_x$. In the above formulation three more scaled parameters have been introduced and they are given by $e = \frac{a}{\epsilon^2 E} \alpha$, $\eta = (\frac{E}{a})^{1/2} \tilde{\eta}$, and $\gamma = \frac{\Gamma \epsilon^2}{Ma^2}$. Furthermore, the coherent spinodal is now located through the variable η and the appropriate time scale for the problem becomes $\tau = \frac{Ma^2}{\epsilon^2} t$. Finally, the Green's function appearing in Eq. (13) must satisfy

$$\nabla^4 G(\mathbf{r}, \mathbf{r}') = \delta(\mathbf{r} - \mathbf{r}'). \quad (14)$$

III. RESULTS

A. Linear stability analysis

A great deal of insight into the interaction between dislocations, irradiation, and spinodal decomposition can be gained by performing a linear stability analysis of Eqs. (12) and (13). Before doing so, however, it is worthwhile discussing some important simplifications. First, we have neglected any defect production term in the equation of motion describing the Burgers vector field. At the early stages of phase separation when the density of cascade-generated vacancy loops is much less than the total dislocation density, this is a reasonable assumption. At later times, however, the assumption may break down. In a future contribution we will investigate in more

detail the role of defect production. Second, in what follows we will assume $m_g = m_c = m_\perp$. Under normal circumstances one would expect the glide mobility to be much greater than that of climb, but under irradiation conditions, due to irradiation hardening and the fact that excess point defects aid in dislocation climb, the relative magnitudes of the two mobility components are unknown. Thus, equal mobilities is not an unreasonable assumption and, as shown below, tractable analytic results can be obtained. Finally, the model assumes that the excess point defect concentrations provide a mechanism for increased dislocation mobility, but annihilation and recombination of vacancies and interstitials is not explicitly included. Therefore effects such as radiation-induced segregation via the inverse Kirkendall effect are not described by the current model.

To proceed with a linear stability analysis, we multiply Eq. (13) by the quantity ∇_y and multiply the corresponding equation describing the kinetics of the b_y field by the term $-\nabla_x$. Addition of the two equations results in a differential equation involving only the function ψ , which is a shorthand notation for $\psi = \nabla^4 X_d$. Furthermore, a linearization of the governing equations yields the following Fourier space representation:

$$\begin{bmatrix} \frac{\partial U}{\partial \tau} \\ \frac{\partial \Psi}{\partial \tau} \end{bmatrix} = \begin{bmatrix} \omega & \eta \\ m_\perp \eta k^2 & -m_\perp(1 + ek^2) \end{bmatrix} \begin{bmatrix} U \\ \Psi \end{bmatrix}, \quad (15)$$

where k is the magnitude of the wave vector and U and Ψ are the Fourier space counterparts of the composition and ψ fields. In Eq. (15) the quantity ω is defined by

$$\omega = k^2(1 - \eta^2) - k^4 - \frac{\gamma \rho^2 k^2}{1 + k^2 \rho^2}, \quad (16)$$

where ρ is the dimensionless cascade radius.

At this point it is interesting to consider the special case in which mobile dislocations instantaneously adjust to the evolving composition field. Mathematically, this can be achieved by taking the limit $m_\perp \rightarrow \infty$ in Eq. (15), with the result that the perturbation growth rate λ for the composition field is given by

$$\lambda = k^2(1 - \eta^2) + \frac{\eta^2 k^2}{1 + ek^2} - k^4 - \frac{\gamma \rho^2 k^2}{1 + k^2 \rho^2}. \quad (17)$$

The second term in Eq. (17) accounts for the presence of dislocations with finite core energy e . It can be seen that in the limit of vanishing e , $\lambda = k^2 - k^4 - \frac{\gamma \rho^2 k^2}{1 + k^2 \rho^2}$, which describes the behavior of the alloy within the *chemical* spinodal under irradiation. That is, infinitely mobile dislocations may relax all coherency misfit strains, in agreement with the analysis in Appendix B. At finite core energy and long wavelengths corresponding to $ek^2 \ll 1$, on the other hand, $\lambda \approx k^2 - \eta^2 ek^4 - k^4 - \frac{\gamma \rho^2 k^2}{1 + k^2 \rho^2}$ to leading order. In this limit, the contribution from the finite core energy can be incorporated into a renormalized surface tension $\Gamma^{\text{eff}} = \Gamma(1 + \eta^2 e)^{1/2}$ which drives the coarsening of the alloy. This simple analysis suggests that phase separation in irradiated alloys is indeed possible at temperatures very close to the chemical spinodal.

Turning to the more general case of finite m_\perp , instability in the system occurs when an eigenvalue of the matrix on the

right-hand side of Eq. (15) is positive. The eigenvalues, λ , are given by

$$2\lambda = (\omega - m_{\perp}[1 + ek^2]) \pm \sqrt{(\omega - m_{\perp}[1 + ek^2])^2 + 4m_{\perp}(1 + \omega + [e + \eta^2]k^2)}. \quad (18)$$

An important result from the linear stability analysis is the fact that for $m_{\perp} \neq 0$ and in the absence of irradiation the system is *always* unstable for all points below the chemical spinodal ($a > 0$) and it is only in the limit of zero dislocation mobility that the Cahn coherent spinodal line is reproduced. However, as shown in the Fig. 1 plot of largest eigenvalue vs wave number k , the growth rate of the fastest growing composition mode varies with m_{\perp} . The solid lines refer to the materials parameters $\eta = 1, e = 0, \rho = 2, \gamma = 1$, and the labels on each curve denote the dislocation mobility. The λ vs k curves increase with increasing mobility and as m_{\perp} tends to infinity the eigenvalue function approaches the case $\eta = 0$ as discussed above. There is, however, an effect due to dislocation core energy as depicted by the dotted line in Fig. 1, which corresponds to the case where the parameter e is increased to 0.2 ($m_{\perp} = 1$). Clearly the effect of increasing core energy is a decrease in the initial amplification rate and a shift of the dominant wavelength to coarser structures.

The dispersion curves of Fig. 1 are qualitatively similar to Cahn's original treatment of spinodal decomposition in that even in the limit of k approaching zero the system is unstable. Under irradiation conditions, however, the phase separation behavior can be quite different. Figure 2 shows (solid lines) the λ vs k relation for the set of parameters $\eta = 1, m_{\perp} = 1$, and $e = 0$, but now the energy of incident irradiation is increased such that $\rho = 2$. Three curves are depicted where, from top to bottom, the flux of energetic particles is increased

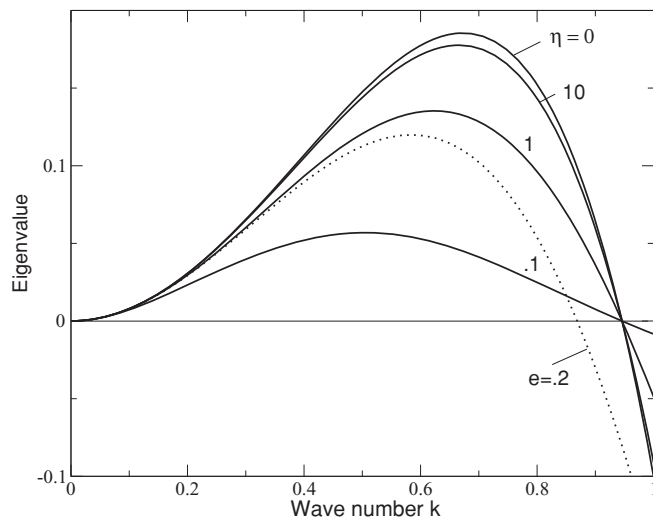


FIG. 1. Solid lines show the dispersion relationship, λ vs k , for an irradiated system with $\rho = 2, \gamma = 1, e = 0, \eta = 1$, and various values of m_{\perp} labeled on each curve. The results demonstrate that instability occurs for all points below the chemical spinodal and with increasing dislocation mobility the dispersion relation approaches that with no coherency strain $\eta = 0$. The dotted line depicts the case when the dislocation core energy is increased to $e = 0.2$.

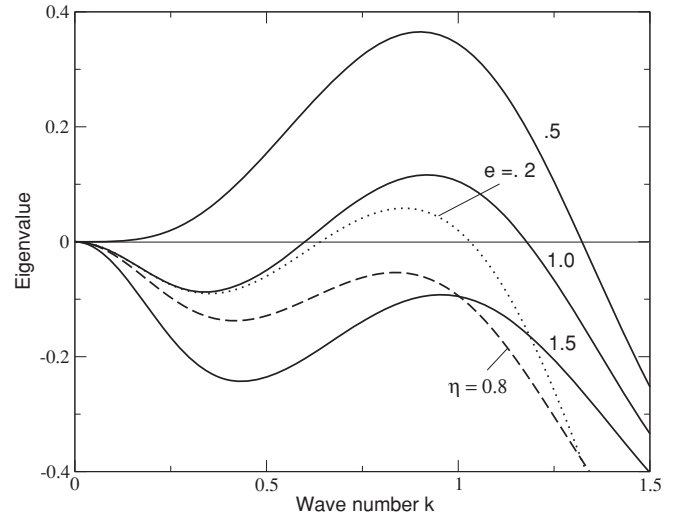


FIG. 2. The solid lines show the dispersion relationship for an irradiated system with $\rho = 2, e = 0$, and $m_{\perp} = 1$. The top curve ($\gamma = 0.5$) illustrates the case where complete phase separation is expected and the bottom curve with $\gamma = 1.5$ depicts irradiation conditions where a homogeneous solid solution is maintained. The intermediate case ($\gamma = 1.5$) shows a dispersion relation suggesting patterning. The change in the dispersion relationship ($\gamma = 1$) with a change in η is depicted by the dashed line and the dotted curve illustrates the change arising from an increase in the dislocation core energy to $e = 0.2$.

and the value of γ is labeled for each line. At relatively low flux ($\gamma = 0.5$) the system is unstable with respect to infinitely long wavelengths and the system is expected to exhibit complete phase separation. For high fluxes (the bottom curve) the ballistic mixing effect is sufficiently vigorous that the system is stable and a homogeneous solid solution is maintained. The intermediate case ($\gamma = 1$) describes a system that is unstable but the instability occurs over a *band* of wave numbers. As explained by Enrique and Bellon, in these cases the competition between the stabilizing effect of ballistic mixing and the thermodynamic tendency to phase separate results in a stable composition pattern characterized by a fixed periodicity and amplitude. For the case of patterning, some Fourier modes will increase in amplitude at an early time, but complete coarsening will be suppressed due to the change in sign of the eigenvalue in the low k regime. It is interesting to note that the qualitative behavior with respect to patterning, phase separation, and complete mixing is unchanged with a change in m_{\perp} . That is, the amplitude of the fastest growing perturbation varies with the dislocation mobility, but the zeros of the dispersion curves remain the same. However, a change in η or e will alter the regimes where patterning is observed. With $\gamma = 1$ and $\rho = 2$, the dashed curve in Fig. 2 illustrates the change in the dispersion relation when η is decreased to 0.8 (notice the system changes from a patterning system to complete stability) and the dotted line shows the behavior as the core energy is increased to 0.2.

The results of Fig. 2 and subsequent discussion suggest a qualitative means of identifying when an irradiated system will exhibit patterning, complete phase separation, or solid-solution tendencies. As pointed out by Enrique and Bellon, in a space of ρ vs γ the locus of points where the first derivative

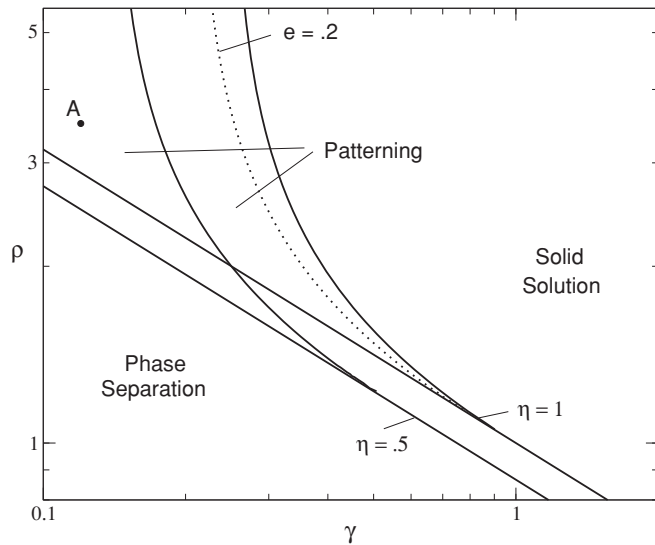


FIG. 3. The Enrique-Bellon plot showing regions in ρ - γ space where complete phase separation, solid solution, and patterning are predicted. Results for $\eta = 1$ and $\eta = 0.5$ are shown. Other parameters are $m_{\perp} = 1$ and $e = 0$. The dashed line shows the change in the patterning–solid-solution boundary when e is increased to 0.2 ($\eta = 1$). The point labeled A denotes the conditions used in the numerical simulation.

of λ with respect to k in the $k \rightarrow 0$ limit equals zero will define the region of complete phase separation. Furthermore, the conditions when a single root of the λ vs k functions is observed at $k \neq 0$ delineates the onset of compositional patterning. Two examples of the Enrique-Bellon plot are depicted in Fig. 3.³⁹ For systems exhibiting a lower atomic size mismatch ($\eta = 0.5$) the onset of patterning behavior shifts to lower values of the incident flux and slightly higher values of the cascade radius ρ . The dashed line in Fig. 3 depicts the shift in the solid-solution–patterning boundary when the dislocation core energy e is increased from 0 to 0.2 (for $\eta = 1$). Clearly, with increasing e there is a decrease in area of the patterning regime resulting from a shift of the solid-solution–patterning boundary to lower γ .

Many of the predictions from the linear stability analysis are consistent with previous experimental studies of irradiation-induced spinodal decomposition. For example, Nakai and Kinoshita¹⁷ have observed, in agreement with theory, that the wavelength of composition modulations in several alloy systems decreases with increasing irradiation flux and increasing temperature. There are, however, observations that unfortunately, appear to be at odds with the model described here. Consider the case of Au-Ni alloys. Nakai *et al.* have observed concentration fluctuations at high temperatures quite close to the chemical spinodal. In this temperature regime the length scale for the composition field becomes very large and hence the scaled cascade radius ρ becomes very small. Moreover, the Nakai experiments employed 0.4–1 MeV electrons, which produces damage cascades of roughly one nearest-neighbor spacing. Since ρ is predicted to be small, according to the stability diagram of Fig. 3, the system cannot exhibit patterning. The discrepancy between theory and experiment can perhaps be traced to the assumptions invoked.

Other than to provide for an increased dislocation mobility, excess point defects do not appear explicitly in the model and it is well known that irradiation-induced point defects can lead to compositional patterns even for alloys that do not phase separate. Thus, we tentatively conclude that the results at high temperatures observed by Nakai *et al.* are not spinodal decomposition in the traditional sense and are more accurately described by the models proposed by Martin^{40,41} and Murphy.⁴²

It is important to stress that the results of Fig. 3 are based on a linear stability analysis and thus provide only a qualitative picture of phase separation in irradiated systems. To provide a more accurate assessment of the evolution of the composition and dislocation density fields, a numerical solution to the governing kinetic equations is required and the results of the nonlinear modeling will be discussed in the next section.

B. Numerical simulations

The main goal of this section is to compare phase-separating microstructures in the absence of irradiation and the patterns which can appear under a flux of energetic particles. A complete survey of the trends observed as a function of materials parameters, such as mobility and coherency strain, is beyond the scope of the present work and will be investigated in future studies. The nonlinear equations of motion in dimensionless form are given by

$$\frac{\partial u}{\partial \tau} = \nabla^2 [-(1 - \eta)u + u^3 - \nabla^2 u] + \eta \psi - \gamma \int d\mathbf{r}' [\delta(\mathbf{r} - \mathbf{r}') - K_0(|\mathbf{r} - \mathbf{r}'|/\rho)] u(\mathbf{r}') \quad (19)$$

and

$$\frac{\partial \psi}{\partial \tau} = -m_{\perp}(\psi + \eta \nabla^2 u - e \nabla^2 \psi). \quad (20)$$

The system of equations was solved in real space using a straightforward explicit time-stepping scheme (see, e.g., Ref. 43). A computational domain consisting of a 200×200 square grid was employed with a grid spacing of $\Delta x = 1$ (results are not changed for smaller values of the grid spacing). The system was evolved starting from Gaussian-distributed small-amplitude random fluctuations about the $u = 0$ and $\psi = 0$ uniform states. For stability a time step of 0.01 was needed. The singular grid point in the convolution integral in Eq. (19) was evaluated by integrating over an equivalent area circle and using the relation $\int r K_0(r) dr = -r K_1(r)$. The upper cutoff to the convolution integral was set at 5ρ , which yielded a value of the integral over the weight function within 2% of the analytic result, and the simulation results were unchanged by using a larger cutoff.⁴⁴

Before investigating the effects of irradiation it is instructive to discuss the phase-separation behavior when there is no flux of incident particles ($\gamma = 0$). The top panel of Fig. 4 depicts the u field over the computational domain after a dimensionless time of $\tau = 1000$ and a quench position given by $\eta = 1$. The regions of high concentration are represented by white (yellow), whereas the black areas correspond to values of $u = -1$. In the $\gamma = 0$ run a dislocation mobility of $m_{\perp} = 1$ was chosen and a core energy of $e = 0.1$ was assumed. The

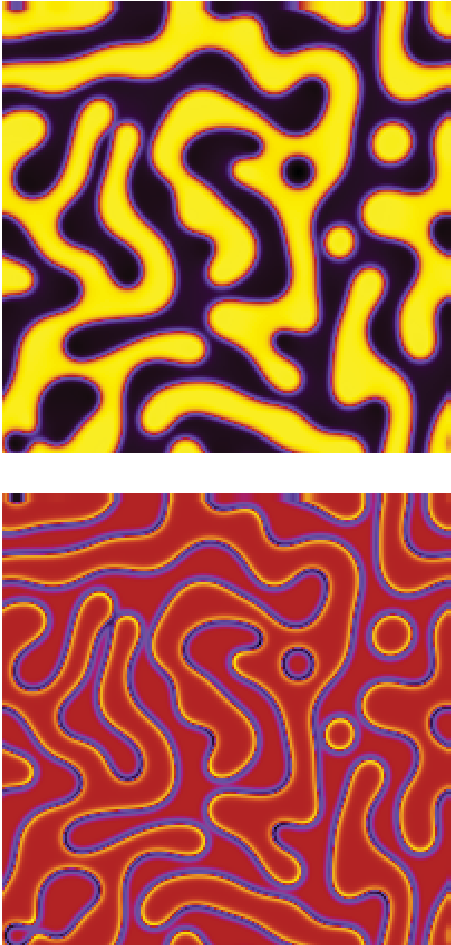


FIG. 4. (Color online) Top: The concentration field u after a dimensionless time of $\tau = 1000$ for the case where no irradiation effects are included. The black areas represent low values of the concentration, whereas white (yellow) corresponds to $u = +1$. Bottom: The function ψ after the same time, where for clarity ψ has been multiplied by a factor of 2. ψ is nearly zero (red) everywhere except at phase boundaries.

bottom panel in the figure shows the function ψ after the same aging time, where for clarity of presentation, the value of ψ has been multiplied by a factor of 2. The important observation here is the fact that ψ is nearly equal to zero (red) everywhere except at the boundaries of the emerging phases. As a phase boundary is traversed, ψ varies from a high positive to a low negative value. Since ψ is defined in terms of the gradients of the dislocation density fields [Eq. (4)], the oscillation near the interfaces indicates that in order to reduce the strain energy due to atomic size mismatch, misfit dislocations have segregated to the boundaries. The segregation effect can perhaps be seen more clearly in Fig. 5, which shows the u and ψ functions plotted along a horizontal slice through the center of the computational box. The coupling between the dislocation (dashed line) and concentration fields (solid line) during the coarsening process is evident. A similar coordinated motion of dislocations and phase boundaries has been observed at the atomic scale in a recent study of the phase field crystal model of a binary alloy.⁴⁵

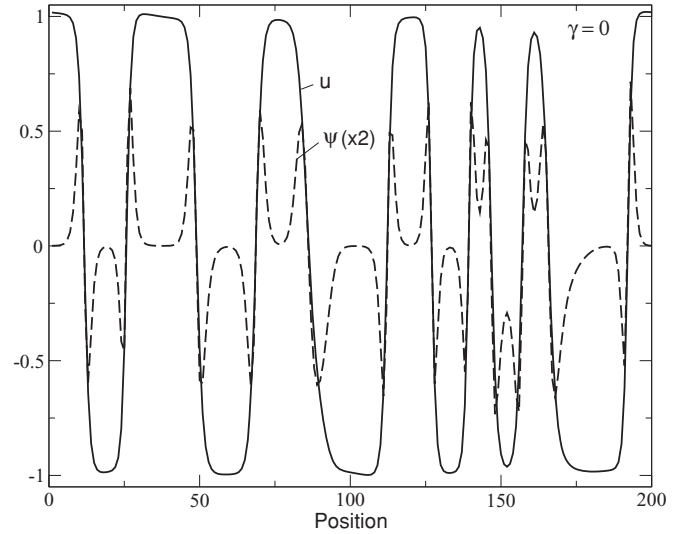


FIG. 5. A slice through the center of the computational domain showing the dislocation and concentration fields as a function of position. The solid line corresponds to the top snapshot depicted in Fig. 4, whereas the dashed line corresponds to the bottom panel.

The effect of irradiation on the phase-separation process can be seen from the u field contour plot shown in Fig. 6. Here the materials parameters are the same as those used for the simulations of Fig. 4 but now the irradiation terms $\rho = 3.5$ and $\gamma = 0.12$ have been employed. The irradiation conditions correspond to the point labeled A in Fig. 3, which lies in the patterning region predicted by linear theory (for $\eta = 1$). The simulation time shown in Fig. 6 is $\tau = 1000$, which is the same as that depicted in the nonirradiation case of Fig. 4, yet the characteristic domain size and the amplitude of the concentration deviation are less than that of the unirradiated phase-separation case. In fact, the u and ψ fields for the irradiated conditions remain virtually unchanged for much longer aging times, indicating the system has reached a state of composition patterning. In addition, the numerical simulations are consistent with the predictions of the

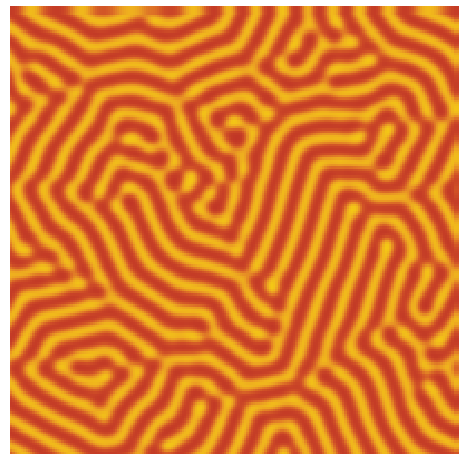


FIG. 6. (Color online) The u field for the case where $\rho = 3.5$ and $\gamma = 0.12$ (the point A in Fig. 3) at a scaled time of $\tau = 1000$. The composition patterning observed is consistent with the prediction of linear theory.

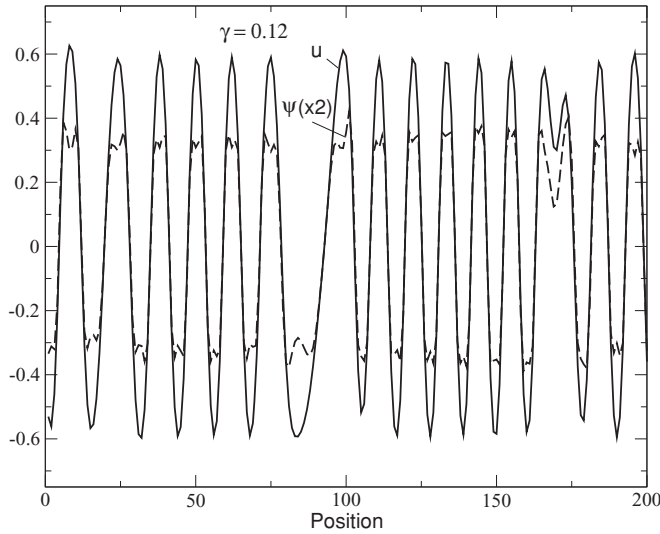


FIG. 7. A cut through the computational domain showing the u and Ψ fields for the patterning case of Fig. 6.

linear stability analysis in the sense that both the amplitude and wavelength of the composition pattern increases as the irradiation conditions move to the left of point A in Fig. 3. The patterned structure shown in Fig. 6 is qualitatively similar to the results of Enomoto *et al.*³⁷ Moreover, the pattern resembles other systems, such as spinodal decomposition coupled with chemical reactions⁴⁶ and the Swift-Hohenberg model,⁴⁷ that exhibit qualitatively similar dispersion curves to the case depicted by the middle function of Fig. 2.

The dislocation density field for the conditions leading to patterning, i.e., point A in the Enrique-Bellon plot, is qualitatively similar to the u field shown in Fig. 6. Therefore the dislocation pattern is more clearly seen in Fig. 7, which is a slice through the center of the computational domain. As in Fig. 5, the solid line represents the u function vs position and the dashed line is ψ scaled by a factor of 2. The u profiles illustrate the decreased amplitude of the concentration field (note the change in scale from Fig. 5), which is indicative of patterning. With respect to the ψ field, here, as in the complete phase-separation case, there is a tendency for misfit dislocations to segregate to the phase boundaries, but now the segregation pattern is sufficiently fine that the dislocation density does not decay completely to zero within the interior of the domains. Perhaps a more accurate description of the microstructure is one in which misfit dislocations are found both at the interface and within each phase, with a difference in sign of the Burgers vector between high and low concentration regions.

IV. CONCLUSIONS

In previous studies of phase separation in alloys under irradiation, two somewhat surprising results were observed. (1) The alloys can exhibit a composition pattern whose amplitude and wavelength are unchanged after long aging times and (2) phase separation can occur at temperatures well above the coherent spinodal. In this work we have shown that by combining the Enrique-Bellon model of spinodal decomposition under irradiation with the Haataja-Leonard

model of mobile dislocations both of these experimental observations can be explained. The combined model consists of coupled kinetic equations describing the evolution of the composition field and the Airy's stress function arising from dislocation-dislocation interaction. A linear stability analysis of the model allows for a qualitative picture of the regions in ρ - γ space where complete phase separation, solid-solution behavior, and patterning are expected. In short, the presence of dislocations facilitates the phase-separation process above the coherent spinodal, while sufficiently energetic irradiation gives rise to compositional patterning. A full nonlinear treatment reveals how misfit dislocations can alleviate the coherency strains arising due to atomic size mismatch even in the compositional patterning regime.

ACKNOWLEDGMENTS

The authors acknowledge several important discussions with N. Provatas and N. Ofori-Opoku. J.J.H. was supported by a Natural Sciences and Engineering Research Council of Canada (NSERC) Discovery grant.

APPENDIX A: TWO-DIMENSIONAL ANALYSIS OF COHERENT MISFIT STRAINS

First, we will reproduce Cahn's theory for coherent spinodal decomposition in two dimensions using mathematical techniques that will be useful when extending the arguments to dislocations. To this end, we write the stress-strain relation as follows:

$$\sigma_{ij} = \frac{E}{1+\nu}(\epsilon_{ij} + \tilde{\eta}c\delta_{ij}) + \frac{\nu E}{(1+\nu)(1-\nu)}(\epsilon_{kk} + 2\tilde{\eta}c)\delta_{ij}, \quad (\text{A1})$$

where again E denotes the (2D) Young's modulus and ν is the Poisson ratio. According to the equation above, stress-free strains are $\epsilon_{xx}^{s-f} = \epsilon_{yy}^{s-f} = -\tilde{\eta}c$ and $\epsilon_{xy}^{s-f} = 0$, while $\epsilon_{ij} = \epsilon_{ij}^{s-f} + \epsilon_{ij}^{el}$ denotes the total strain (i.e., stress-free strain plus elastic strain). Assuming that the displacement field \mathbf{u} is irrotational ($\nabla \times \mathbf{u} = 0$), we can define a function W such that $\mathbf{u} = \nabla W$, which implies that the total strains satisfy $\epsilon_{ij} = \partial^2 W / (\partial x_i \partial x_j)$. Mechanical equilibrium equations then imply that

$$\nabla^2 W = -\tilde{\eta}(1+\nu)c, \quad (\text{A2})$$

or from the definition of the strains

$$\epsilon_{ij} = -\tilde{\eta}(1+\nu)\nabla^{-2} \frac{\partial^2 c}{\partial x_i \partial x_j}, \quad (\text{A3})$$

where ∇^{-2} denotes the inverse Laplacian.⁴⁸

Now, the elastic strain tensor can be written

$$\overleftrightarrow{\epsilon}^{el} = \begin{bmatrix} -\tilde{\eta}(1+\nu)\nabla^{-2} \frac{\partial^2 c}{\partial x^2} + \tilde{\eta}c & -\tilde{\eta}(1+\nu)\nabla^{-2} \frac{\partial^2 c}{\partial x \partial y} \\ -\tilde{\eta}(1+\nu)\nabla^{-2} \frac{\partial^2 c}{\partial x \partial y} & -\tilde{\eta}(1+\nu)\nabla^{-2} \frac{\partial^2 c}{\partial y^2} + \tilde{\eta}c \end{bmatrix}, \quad (\text{A4})$$

while the corresponding elastic stress tensor becomes

$$\overleftrightarrow{\sigma} = \begin{bmatrix} E(-\tilde{\eta}\nabla^{-2}\frac{\partial^2 c}{\partial x^2} + \tilde{\eta}c) & -\tilde{\eta}(1+\nu)\nabla^{-2}\frac{\partial^2 c}{\partial x\partial y} \\ -\tilde{\eta}(1+\nu)\nabla^{-2}\frac{\partial^2 c}{\partial x\partial y} & E(-\tilde{\eta}\nabla^{-2}\frac{\partial^2 c}{\partial y^2} + \tilde{\eta}c) \end{bmatrix}. \quad (\text{A5})$$

The elastic energy corresponding to these deformations can be written as

$$F_{el} = \frac{1}{2} \int d\mathbf{r} [\sigma_{xx}\epsilon_{xx}^{el} + \sigma_{yy}\epsilon_{yy}^{el} + 2\sigma_{xy}\epsilon_{xy}^{el}], \quad (\text{A6})$$

or

$$F_{el} = \frac{(1+\nu)}{2} \tilde{\eta}^2 E \int d\mathbf{r} \left[\left(\nabla^{-2} \frac{\partial^2 c}{\partial x^2} \right)^2 + \left(\nabla^{-2} \frac{\partial^2 c}{\partial y^2} \right)^2 + 2 \left(\nabla^{-2} \frac{\partial^2 c}{\partial x\partial y} \right)^2 - \frac{\nu c^2}{(1+\nu)} \right]. \quad (\text{A7})$$

It is straightforward to demonstrate in a Fourier representation that

$$\int d\mathbf{r} \left[\left(\nabla^{-2} \frac{\partial^2 c}{\partial x^2} \right)^2 + \left(\nabla^{-2} \frac{\partial^2 c}{\partial y^2} \right)^2 + 2 \left(\nabla^{-2} \frac{\partial^2 c}{\partial x\partial y} \right)^2 \right] = \int d\mathbf{r} c^2. \quad (\text{A8})$$

Therefore, the elastic energy due to coherency strains in an isotropic 2D system is given by the simple expression

$$F_{el} = \frac{1}{2} \tilde{\eta}^2 E \int d\mathbf{r} c^2, \quad (\text{A9})$$

which appears in the free expression given by Eq. (2).

APPENDIX B: COUPLING BETWEEN DISLOCATIONS AND COHERENCY STRAINS

To incorporate misfit dislocations in the analysis above, we first write the net elastic energy $F_{el} = 1/2 \int d\mathbf{r} \sigma_{ij} \epsilon_{ij}^{el}$ in terms of singular (i.e., those due to dislocations) and nonsingular (those due to coherency stresses) pieces:

$$F_{el} = \frac{1}{2} \int d\mathbf{r} (\sigma_{ij}^s + \sigma_{ij}^{ns}) (\epsilon_{ij}^{el;s} + \epsilon_{ij}^{el;ns}) \\ = F_{el}^{ns} + F_{el}^s + F_{\text{coupl}}, \quad (\text{B1})$$

where $F_{el}^{ns} = \frac{1}{2} \int d\mathbf{r} \sigma_{ij}^{ns} \epsilon_{ij}^{el;ns} = \frac{1}{2} \tilde{\eta}^2 E \int d\mathbf{r} c^2$ from Eq. (A9), $F_{el}^s = \frac{1}{2E} \int d\mathbf{r} (\nabla^2 \chi)^2$ and $\sigma_{ij}^s = \epsilon_{ik} \epsilon_{jl} \nabla_k \nabla_l \chi$ with ϵ denoting the antisymmetric tensor ($\epsilon_{xx} = \epsilon_{yy} = 0$ and $\epsilon_{xy} = -\epsilon_{yx} = 1$), and the coupling $F_{\text{coupl}} = \int d\mathbf{r} \epsilon_{ij}^{el;ns} \sigma_{ij}^s$. Upon employing the elastic coherency strains from Eq. (A4), we obtain

$$F_{\text{coupl}} = \tilde{\eta} \int d\mathbf{r} c \nabla^2 \chi + \tilde{\eta}(1+\nu) \int d\mathbf{r} \left[-\frac{\partial^2 \chi}{\partial y^2} \nabla^{-2} \frac{\partial^2 c}{\partial x^2} - \frac{\partial^2 \chi}{\partial x^2} \nabla^{-2} \frac{\partial^2 c}{\partial y^2} + 2 \frac{\partial^2 \chi}{\partial x \partial y} \nabla^{-2} \frac{\partial^2 c}{\partial x \partial y} \right]. \quad (\text{B2})$$

It is straightforward to show by using a Fourier representation that the last term in Eq. (B2) integrates to zero, and thus

$$F_{\text{coupl}} = \tilde{\eta} \int d\mathbf{r} c \nabla^2 \chi. \quad (\text{B3})$$

Finally, we note that F_{el} is minimized when dislocations completely relax the coherency strains.

¹G. S. Was, *Fundamentals of Radiation Materials Science* (Springer-Verlag, Berlin, 2007), pp. 433–490.

²K. Bertram, F. J. Minter, J. A. Hudson, and K. C. Russell, *J. Nucl. Mater.* **75**, 42 (1978).

³M. R. Mruzik and K. C. Russell, *J. Nucl. Mater.* **78**, 343 (1978).

⁴R. S. Nelson, J. A. Hudson, and D. J. Mazey, *J. Nucl. Mater.* **44**, 318 (1972).

⁵P. Wilkes, *J. Nucl. Mater.* **83**, 166 (1979).

⁶A. D. Brailsford, *J. Nucl. Mater.* **91**, 221 (1980).

⁷H. J. Frost and K. C. Russell, *Acta Metall.* **30**, 953 (1982).

⁸C. Abromeit, V. Naundorf, and H. Wollenberger, *J. Nucl. Mater.* **155–157**, 1174 (1988).

⁹K. C. Russell, *J. Nucl. Mater.* **83**, 176 (1979).

¹⁰R. Cauvin and G. Martin, *Phys. Rev. B* **23**, 3333 (1981).

¹¹R. Cauvin and G. Martin, *Phys. Rev. B* **23**, 3322 (1981).

¹²F. Haider, P. Bellon, and G. Martin, *Phys. Rev. B* **42**, 8274 (1990).

¹³F. Soisson, P. Bellon, and G. Martin, *Phys. Rev. B* **46**, 11332 (1992).

¹⁴G. Martin and P. Bellon, *Solid State Phys.* **50**, 189 (1996).

¹⁵W. Wagner, R. Poerschke, and H. Wollenberger, *J. Phys. F* **12**, 405 (1982).

¹⁶F. A. Garner, J. M. McCarthy, K. C. Russell, and J. J. Hoyt, *J. Nucl. Mater.* **205**, 411 (1993).

¹⁷K. Nakai and C. Kinoshita, *J. Nucl. Mater.* **169**, 116 (1989).

¹⁸K. Nakai, C. Kinoshita, and N. Nishimura, *J. Nucl. Mater.* **179–181**, 1046 (1991).

¹⁹Y. Asai, Y. Isobe, K. Nakai, C. Kinoshita, and K. Shinohara, *J. Nucl. Mater.* **179–181**, 1050 (1991).

²⁰M. Haataja and F. Leonard, *Phys. Rev. B* **69**, 081201 (2004).

²¹M. Haataja, J. Muller, A. D. Rutenberg, and M. Grant, *Phys. Rev. B* **65**, 165414 (2002).

²²M. Haataja, J. Mahon, N. Provatas, and F. Leonard, *Appl. Phys. Lett.* **87**, 251901 (2005); M. Haataja, J. Muller, A. D. Rutenberg, and M. Grant, *Phys. Rev. B* **65**, 165414 (2002).

²³F. Leonard and M. Haataja, *Appl. Phys. Lett.* **86**, 181909 (2005).

²⁴R. A. Enrique and P. Bellon, *Phys. Rev. Lett.* **84**, 2885 (2000).

²⁵R. A. Enrique and P. Bellon, *Phys. Rev. B* **63**, 134111 (2001).

²⁶R. A. Enrique and P. Bellon, *Phys. Rev. B* **70**, 224106 (2004).

²⁷R. A. Enrique and P. Bellon, *Appl. Phys. Lett.* **78**, 4178 (2001).

²⁸R. A. Enrique, K. Nordlund, R. S. Averbach, and P. Bellon, *J. Appl. Phys.* **93**, 2917 (2003).

²⁹J. W. Cahn and J. E. Hilliard, *J. Chem. Phys.* **28**, 258 (1958).

³⁰J. W. Cahn, *Acta Metall.* **9**, 795 (1961).

³¹J. J. Hoyt, *Phase Transformations* (McMaster Innovation Press, Hamilton, ON, 2010).

³²D. R. Nelson, *Phys. Rev. B* **18**, 2318 (1978).

³³D. R. Nelson and B. I. Halperin, *Phys. Rev. B* **19**, 2457 (1979).

³⁴B. Bako and W. Hoffelner, *Phys. Rev. B* **76**, 214108 (2007).

³⁵I. Groma and B. Bako, *Phys. Rev. Lett.* **84**, 1487 (2000).

³⁶Y. Enomoto and S. Iwata, *Surf. Coat. Technol.* **169–170**, 233 (2003).

³⁷Y. Enomoto and M. Sawa, *Metall. Trans. A* **43**, 641 (2002).

³⁸Determination of the variational derivative of the free energy with respect to b_x is not entirely straightforward. Details of the procedure can be found in Appendix B of Ref. 21.

³⁹We have employed a slightly different set of scaled variables and thus the γ axis of Fig. 3 differs from that of Enrique and Bellon by a factor of $\sqrt{2}$.

⁴⁰G. Martin, *Phys. Rev. B* **21**, 2122 (1980).

⁴¹C. Abromeit and G. Martin, *J. Nucl. Mater.* **271-272**, 251 (1999).

⁴²S. M. Murphy, *Metall. Trans. A* **20A**, 2599 (1989).

⁴³T. M. Rogers, K. R. Elder, and R. C. Desai, *Phys. Rev. B* **37**, 9638 (1988).

⁴⁴An approximate correction for the upper cutoff can be formulated as follows. Let Σ represent the integral of the weight function up

to the specified cutoff. An addition term of the form $-\gamma(1 - \Sigma)\bar{u}$, where \bar{u} is the overall average of the composition in the system, can then be added to the right-hand side of the equation of motion for u . The correction is very small but prevents a long time drift in the average concentration away from the correct value of $\bar{u} = 0$.

⁴⁵K. R. Elder, N. Provatas, J. Berry, P. Stefanovic, and M. Grant, *Phys. Rev. B* **75**, 064107 (2007).

⁴⁶S. C. Glotzer, E. A. Di Marzio, and M. Muthukumar, *Phys. Rev. Lett.* **74**, 2034 (1995).

⁴⁷N. Provatas and K. R. Elder, *Phase Field Methods in Materials Science* (Wiley-ICH, Weinheim, 2010).

⁴⁸Note that $\nabla^{-2}h(\mathbf{r}) \equiv \int d\mathbf{r}' G(\mathbf{r} - \mathbf{r}')h(\mathbf{r}')$, where the Green's function satisfies $\nabla^2 G = \delta(\mathbf{r} - \mathbf{r}')$.